Journal of Inorganic and Organometallic Polymers and Materials (2022) 32:728–740
https://doi.org/10.1007/s10904-021-02132-9

Gamma Irradiation Assisted the Sol–Gel Method for Silver Modified-Nickel Molybdate Nanoparticles Synthesis: Unveiling the Antimicrobial, and Antibiofilm Activities Against Some Pathogenic Microbes

M. I. A. Abdel Maksoud[1] · Gharieb S. El-Sayyad[2] · Eman Fayad[3] · Amal Alyamani[3] · Ola A. Abu Ali[4] · Aliaa A. Elshamy[5]

Received: 12 September 2021 / Accepted: 13 October 2021 / Published online: 19 October 2021

Abstract

Herein, this work aims to reveal the gamma irradiation-assisted the sol–gel method for the synthesis of silver (Ag) modified-nickel molybdate nanoparticles ($NiMoO_4$; NMO NPs) and tested for their antimicrobial and antibiofilm activities against some pathogenic bacteria and unicellular fungi. The prepared samples were characterized via XRD, HR-TEM, SEM, EDX, and elemental mapping analysis. The antimicrobial potential was tested as ZOI and MIC, while antibiofilm was estimated by tube method. The detected diffraction peaks of bare NMO NPs affirmed the successful synthesis of NMO NPs without any foreign phases. Also, three diffraction peaks were detected affirming the formation of Ag NPs on the surface of NMO NPs. The average crystallite size for the bare NMO NPs and Ag@NMO NPs was found to be 71.8 nm and 48.28 nm, respectively. Also, the SEM images have illustrated the decoration of Ag NPs on the NMO surface. Further, the TEM image illustrated that the particles of NMO possess a hexagonal shape in the nanoscale regime. Also, the elemental mapping images confirm the uniform distribution of these elements over the Ag@NMO sample. Antimicrobial results revealed that the synthesized Ag@NMO NPs recorded the most significant inhibition zone more than NMO NPs against *Enterococcus columbae* (33.3 ± 0.115 mm), and *Candida albicans* (30.8 ± 0.572 mm), and the lowest MIC (0.048 µg/ml) against *E. columbae*. Antibiofilm activity of Ag@NMO NPs recording 94.32% for *E. columbae*, 91.99% for *S. vitulinus*, and 90.98% for *C. albicans*. SEM imaging in the lack of Ag@NMO NPs exhibited normally grown bacterial cells with standard typical semi-formed biofilm. After Ag@NMO NPs treatment, remarkable morphological changes; including the total lysis of the outer surface attended by deformations with the reduction in the whole viable number.

Keywords Ag modified-$NiMoO_4$ nanoparticles · *Enterococcus columbae* · Reaction mechanism · Antimicrobial activity · Antibiofilm potential

M. I. A. Abdel Maksoud and Gharieb S. El-Sayyad have contributed equally to this work.

✉ M. I. A. Abdel Maksoud
muhamadmqsod@gmail.com

✉ Gharieb S. El-Sayyad
Gharieb.S.Elsayyad@eaea.org.eg

[1] Materials Science Lab., Radiation Physics Department, National Center for Radiation Research and Technology (NCRRT), Egyptian Atomic Energy Authority (EAEA), Cairo, Egypt

[2] Drug Microbiology Lab., Drug Radiation Research Department, National Center for Radiation Research and Technology, Egyptian Atomic Energy Authority (EAEA), Cairo, Egypt

[3] Department of Biotechnology, Faculty of Sciences, Taif University, P.O. Box 11099, Taif 21944, Saudi Arabia

[4] Department of Chemistry, College of Sciences, Taif University, P.O. Box 11099, Taif 21944, Saudi Arabia

[5] Department of Microbiology and Immunology, Faculty of Pharmacy, Heliopolis University for Sustainable Development, Cairo, Egypt

1 Introduction

Disorders caused by viral infection [1, 2], mutations [3], and further environmental factors [1, 4], such as tumour [5], and diabetes [6] are performing a critical difficulty for people. Therefore, the increasing bacterial defense to practically all recognized types of traditional antibiotics and the slightly greater bacterial infection have achieved important notification across the past decade [7, 8]. Identifying different approaches for primary development and prevention of diseases is highly important [8–10]. Nanotechnology was adopted to use nanomaterials with small size and more significant surface areas concerning their bulk equivalents [11–13]. The pathogenic bacteria that quickly resist the related antibiotics are *Escherichia coli* and *Staphylococcus aureus*. They were unique species of bacteria that were obtained directly from the intestinal area of animals. *E. coli* and *S. aureus* contributes to an enteric infection, and various species produce other intestinal disorders [14]. Many nanoparticles (NPs) were examined for their antimicrobial potential by applying the agar-disc diffusion process [7, 15]. The benefits of inorganic NPs are the powerful surface-to-volume ratio, many unusual features, and their nano-scale, which promotes actions to connect over the actual organisms like pathogenic fungi, bacteria, and unicellular yeast [16–18].

Recently, the binary metal molybdates ($RMoO_4$; R=Nickel, Cobalt, Zinc, etc.) possess outstanding features that make them excellent materials in critical applications such as energy storage [19], corrosion resistance [20], sensors [21], water remediation [22], antimicrobial agents [23], and water splitting applications [24]. Among them, $NiMoO_4$ (NMO) NPs possess the intense of researchers attributable to their merits such as extraordinary electric conduction, exceptional chemical stability, cost-effective [25], improved electrochemical display [26], photo-luminescence [27], magnetic behavior [28], optical, and photodegradation characteristics [29].

Also, between the NPs that applied in broad areas, silver (Ag) NPs have been distinctly utilized in many applications attributable to their outstanding characteristics such as antibacterial [30], antiviral [31], and antifungal activities [32], anti-inflammatory [33], and anticancer [34, 35]. In addition, nanomaterials showed promising antimicrobial abilities against various pathogenic microorganisms-forming biofilms [16]. The formed biofilms are networks of multi-cellular threads protecting these microorganisms from applied drugs [36–38].

Radiation-induced synthetic techniques, especially those that employ gamma rays combined with solvents, may have favorable characteristics and exceptional choices that make them prevail over their competitors from conventional procedures [39, 40]. The preference for this method is due to its ease of preparation, uncomplicated controllable on size, limited procedures for obedience, environmentally friendly to precursors and solvents [41, 42]. Recently, Abdel Maksoud et al. [43], have studied the antibacterial and antibiofilm activities of Ag@ zinc ferrite NPs against some pathogenic bacteria.

Accordingly, for the first time, this paper listed the gamma irradiation supported the sol–gel process for the construction of Ag modified-NMO NPs (Ag@NMO). Then, the pure NMO NPs, and Ag modified-NMO NPs were examined toward pathogenic strains separated from surgical rooms. The integrated Ag modified-NMO NPs were used as antimicrobial and antibiofilm factors against pathogenic bacteria. So, we assume that the organized NMO NPs, and Ag modified-NMO NPs can be applied for various purposes for biomedical and industrial applications.

2 Materials and Methods

2.1 Materials

Nickel(II) nitrate hexahydrate ($Ni(NO_3)_2{\cdot}6H_2O$), ammonium molybdate ($(NH_4)_2MoO_4$), and silver nitrate ($AgNO_3$) were chosen as source material for Ni, Mo, and Ag, respectively. At the same time, citric acid monohydrate ($C_6H_8O_7$, 99.57%), and ethylene glycol ($C_2H_6O_2$, 99.8%) were used in the synthesis of NMO NPs via a sol–gel method [10, 44–47]. All chemicals were obtained from Sigma-Aldrich (UK) and used as received in the solid-state.

2.2 Preparation of NMO NPs

The NMO NPs were synthesized via the facile sol–gel technique as follows [10, 44–48]. 0.1 M of $Ni(NO_3)_2{\cdot}6H_2O$ and 0.1 M of $(NH_4)_2MoO_4$ were taken in different beakers containing 40 ml di-ionized water. These aqueous solutions were mixed dropwise with the aid of magnetic stirring for 30 min to form a greenish-yellow precipitate (solution A). Further, the stoichiometric ratio of citric acid (in a molar ratio of 1:1 to the precursor metal salts) was dissolved in 40 ml of ionized water under magnetic stirring for 30 min (solution B). Then, solution B was added dropwise to solution A and accompanied by the addition of ethylene glycol (10 ml) as a polymerization promoter to begin the gel formation [49]. The resulting solution ultrasonic irradiation for 45 min where the reaction temperature was reached 80 °C at the end of the sonochemical process [28]. Then, the produced solution was dried (at 400 °C) to initiate the gel formation.

Finally, the dried gel was cooled to room temperature and ground to obtain NMO powder. The resulted NMO powder was washed by water and ethanol several times and collected by centrifugation (4000 rpm for 10 min). The NMO powder dried at 900 °C via utilizing a muffle furnace [10, 50].

2.3 Preparation of Ag Modified-NMO NPs

5 g of pure NMO NPs was mixed with 0.25 g of $AgNO_3$ and dispersed in deionized water. Further, the resulting suspension solutions were mixed under ultrasonic irradiation for 45.0 min. Finally, the mixture solution was subjected to 50.0 kGy at a dose rate of 1.1 kGy/h at ambient conditions. The irradiation was conducted employing Co^{60} gamma-cell sources [43, 51, 52]. After filtration and washing by a mixture of water/ethanol several times, the final product was collected by centrifugation (4000 rpm for 10 min). Then, the powder was dried in a vacuum at 60 °C to give Ag modified-NMO (Ag@NMO) NPs.

2.4 Characterization of Ag@NMO NPs

The pure NMO NPs and Ag-coated NMO NPs were examined via employing the energy dispersive X-ray analysis spectra (EDAX), high-resolution transmission electron microscopy (HRTEM), X-ray diffraction technique (XRD), scanning electron microscopy (SEM), and SEM-EDX mapping analysis [53, 54].

2.5 Antimicrobial Potential of Pure NMO NPs and Ag Modified-NMO NPs

The tested pathogenic bacteria and unicellular fungi were separated from medical places and identified in our published articles [44]. They were *Staphylococcus sciuri*, *Staphylococcus vitulinus*, *Staphylococcus aureus*, *Enterococcus columbae*, *Staphylococcus lentus*, *Candida tropicalis*, *and Candida albicans*, which were helpful taken from Microbiology Lab., NCRRT, Cairo, Egypt. All the examined bacteria and unicellular fungi were maintained on nutrient agar slants at 5 °C for another usage [55]. Well diffusion method was used to estimate the impacts of pure NMO NPs and Ag@NMO NPs on the examined bacteria and unicellular fungi [56]. To investigate the antimicrobial effect of pure NMO NPs and Ag@NMO NPs applying the well diffusion assay, bacterial and *Candida* suspension was developed and set to standard 0.5 McFarland's concentration equal to $(1–3)\times10^8$ CFU/mL. The examined bacteria and unicellular fungi were swapped on a nutrient agar medium. Then 6.0 mm wells were cut on each nutrient agar plate outside and loaded by 50 µL of the examined treatments, and Amoxicillin (AX) and Nystatin (NS) as a positive control. All the tests were done in triplicates, and the tested plates were incubated overnight at 37 °C [57]. The microbial cloud lack of growth was described as a zone of inhibition (ZOI) in mm.

2.6 Minimum Inhibitory Concentration (MIC) Analysis of Pure NMO NPs and Ag@NMO NPs

The well distribution assay determined MIC of pure NMO NPs and Ag@NMO NPs upon the examined bacterial and *Candida* strains [58]. The overnight examined cultures were incubated for 3.0 h at 37 °C. Following that, the inoculum of the established bacteria and unicellular fungi was set to 0.5 McFarland. A complete volume of 50 µL of bacterial and *Candida* suspension was injected into nutrient agar medium plates. Pure NMO NPs and Ag@NMO NPs were serially diluted two-fold with sterile distilled water to varying concentrations (as µg/mL) then set separately in 6.0 mm wells formed on the agar plate's surface. The examined plates were incubated overnight at 37 °C, and the ZOI was assessed in mm. MIC was determined as the most negligible concentration of pure NMO NPs and Ag@NMO NPs that will hinder the possible extension of bacteria and *Candida* following 24 h incubation [59].

2.7 Antibiofilm Determination of Pure NMO NPs and Ag@NMO NPs

Pure NMO NPs and Ag@NMO NPs were examined for their antibiofilm potential toward the tested bacteria and *Candida* species by tubes method [60]. The examined test tubes, including 5.0 mL of the nutrient broth, were mixed with 10 µL of 0.5 McFarland ($1–3\times10^8$ CFU/ml) of the tested bacteria and *Candida* species. Moreover, 0.25 mL of examined pure NMO NPs and Ag@NMO NPs was included in the tubes while the equivalent volume of water was combined with the control tubes. The prepared tubes were incubated overnight at 37 °C. Next to the incubation, the media in the tubes were excluded. The tubes were mixed with phosphate buffer saline (PBS; pH 7) and subsequently dehydrated [61]. About 5.0 mL of sodium acetate (3.0%) was applied for 10 min to maintain the adherent bacteria and *Candida* species, which were rinsed with deionized water [62]. The bacteria and *Candida* biofilms were dyed with crystal violet (CV; 0.1%) for

20 min and washed with deionized water. Subsequently, 3.0 mL ethanol was combined to terminate the CV. The biofilms were quantitatively determined by UV–Visible spectrophotometer (570 nm). The inhibition percentage was assessed by (Eq. 1) [63].

$$\text{Inhibition } \% = \frac{\text{ODc} - \text{ODt}}{\text{ODc}} \times 100 \quad (1)$$

where; OD_c: The absorbance of the control sample (without treatment), OD_t: The absorbance of the treated samples.

2.8 Reaction Mechanism Estimation by SEM

The tested bacterial and *Candida* cells were washed with PBS and flooded with 3.5% glutaraldehyde. The maintained bacterial and candida cells were rinsed regularly with PBS and cleaned with ethanol for 20.0 min at 24 °C before drying. Eventually, the bacterial and *Candida* cells were installed and set above the aluminium pieces to begin the SEM imaging [64]. The treated bacterial and *Candida* cells' morphological and surface characteristics with the tested Ag@NMO NPs had identified by SEM (ZEISS), and comparing with control samples [65].

2.9 Statistical Analysis

The statistical estimate of our results was conducted using the ONE WAY ANOVA (at $P < 0.05$) and decided to be Duncan's multiple varieties studies and the least significant difference (LSD) report [57]. The results and data were analyzed and inquired by SPSS software version 15.

3 Results and Discussion

3.1 Structural Analyses

Figure 1 (A&B) exhibited the EDX spectra of NMO and Ag modified-NMO (Ag@NMO) NPs. The figure confirms the presence of all fundamental elements with a stoichiometric ratio. The EDX spectra are included several peaks such as Ni, Mo, O, and Ag, which affirm the existence of NMO and Ag@NMO NPs [66].

XRD patterns of both the bare NMO NPs and Ag@NMO NPs are displayed in Fig. 2. The detected diffraction peaks of bare NMO NPs belonged with the (JCPDS cards No: 01–086-0361) and affirmed the successful synthesis of NMO NPs without any foreign phases [66–68]. While, for Ag@NMO sample, it is illustrated that the intensity of the detected NMO's peaks was declined. This may be attributable to Ag coating over the NMO surface. Also, the figure confirms the presence of Ag NPs on the Ag@NMO sample. Three diffraction peaks were detected at $2\theta = 38.44°$, 44.51°, and 64.49° (denoted by *) that affirming the formation of Ag NPs (Fig. S1) [69, 70]. Further, the figure illustrated that the peaks were shifted to lower for Ag@NMO sample [71]. This means the increase in the lattice constant of Ag@NMO NPs attributable to the effect of gamma irradiation besides the decoration with Ag NPs [72–74]. The average crystallite size (D) for the bare NMO NPs and Ag@NMO NPs was estimated via Scherrer' equation and is found to be 71.8 nm, and 48.28 nm respectively [75, 76].

Figure 3 shows the HRTEM images of NMO and Ag@NMO NPs. Figure 3A exhibits that the particles of NMO possess a hexagonal shape in the nanoscale regime. Also,

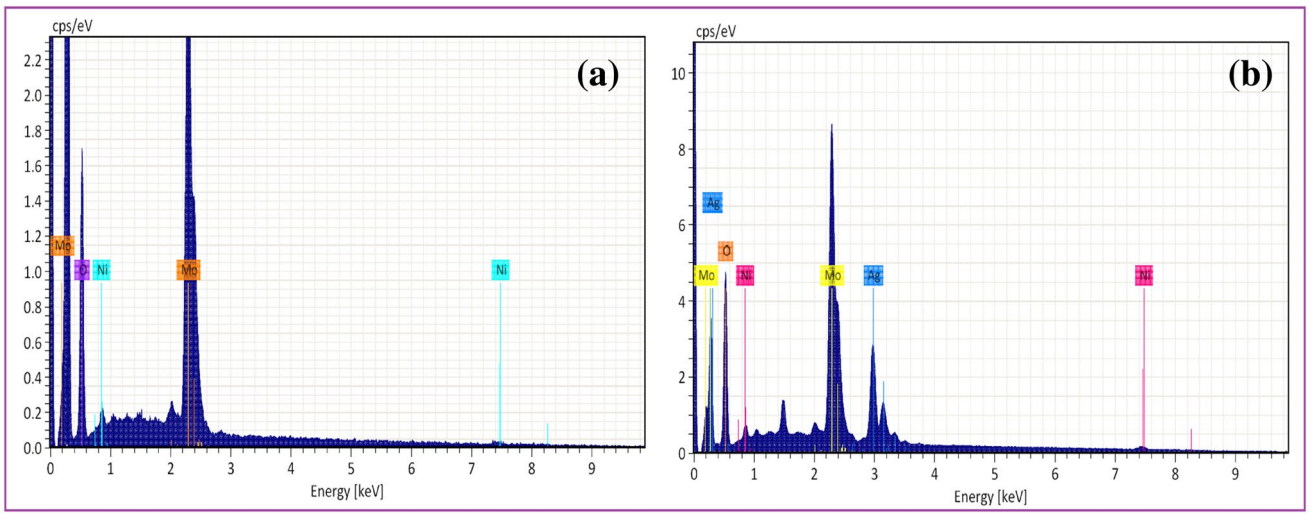

Fig. 1 EDX spectra of **A** pure NMO NPs, and **B** Ag@NMO NPs

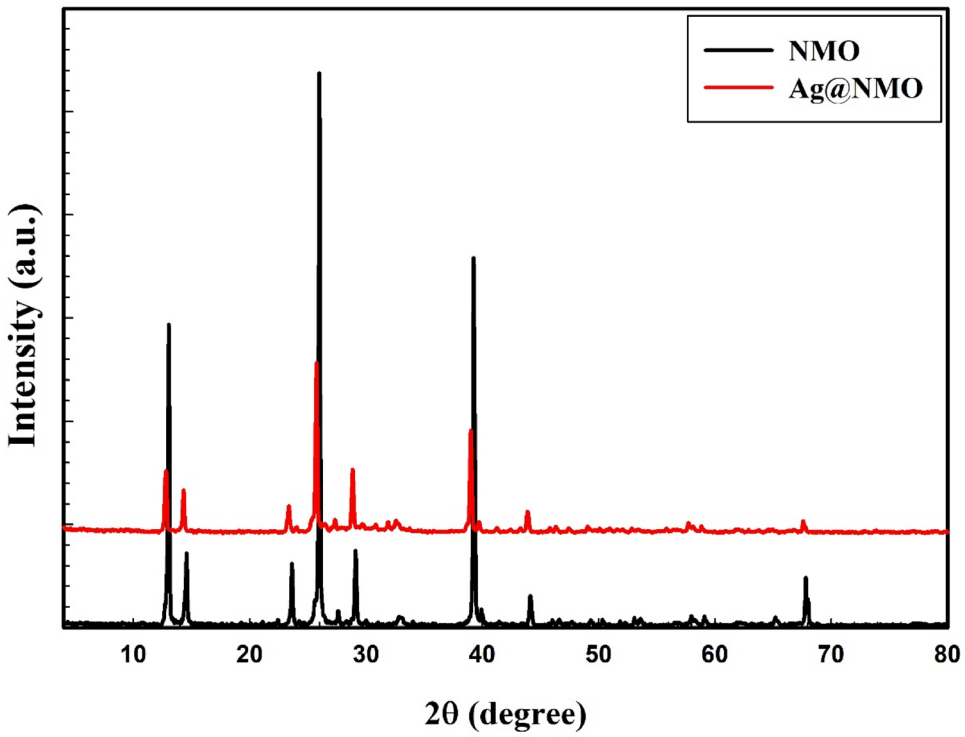

Fig. 2 XRD patterns of pure NMO NPs and Ag@NMO NPs

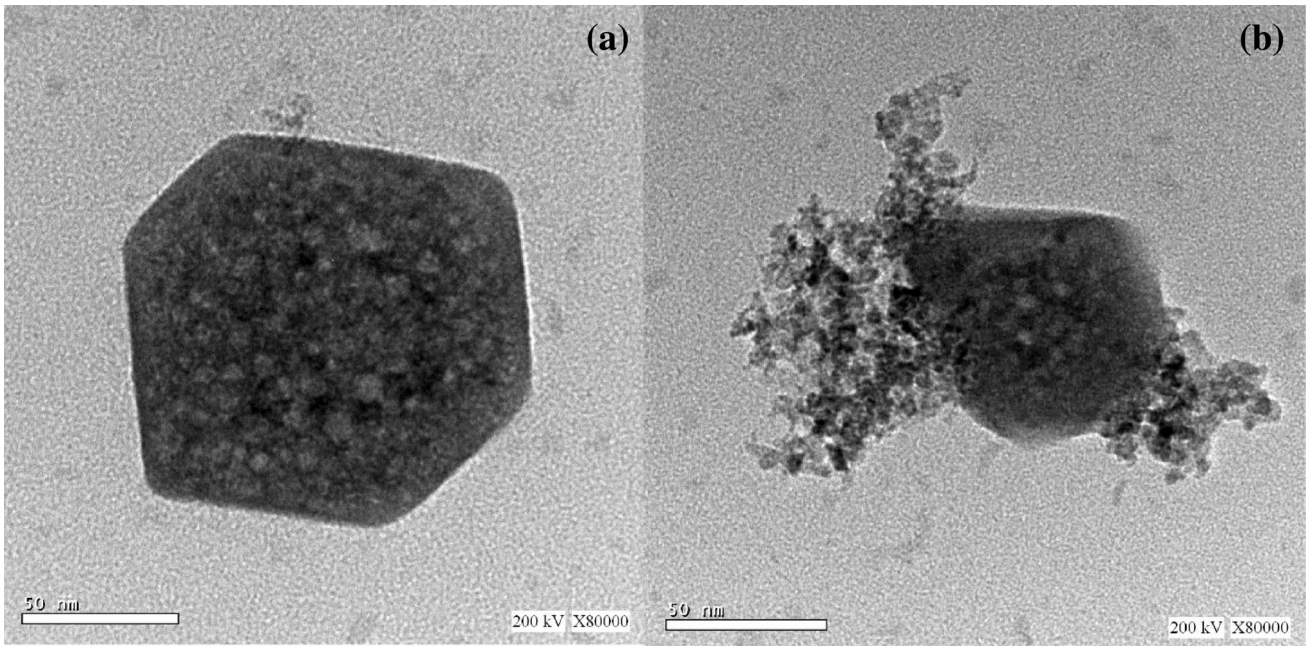

Fig. 3 HRTEM images of **A** pure NMO NPs, and **B** Ag@NMO NPs

Fig. 3B displayed that the particles of Ag modified (as bright particles) on the surface of the hexagonal NMO.

Figure 4 presents the SEM images of pure NMO NPs and Ag@NMO NPs. Figure 4A confirmed that the pure NMO NPs have a nanoplate shape. At the same time, Fig. 4B illustrated the decoration of Ag nanorods on the NMO nanoplate.

Also, the mapping images confirm the presence of Ni, Mo, O, and Ag elements. Besides, the uniform distribution of these elements over the Ag@NMO sample was affirmed in Fig. 5 [77].

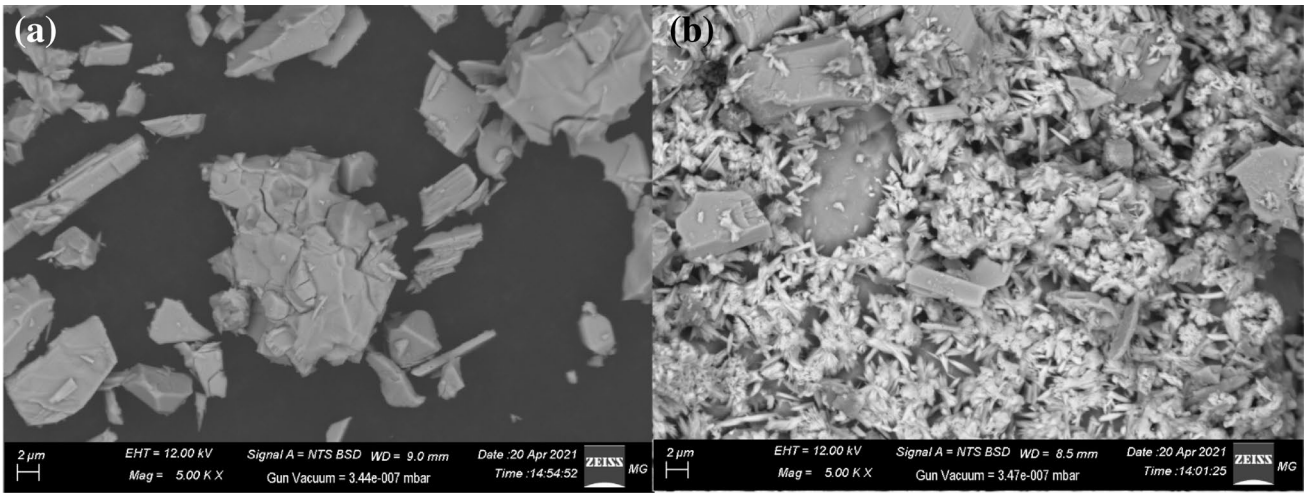

Fig. 4 SEM images of **A** pure NMO NPs and **B** Ag@NMO NPs

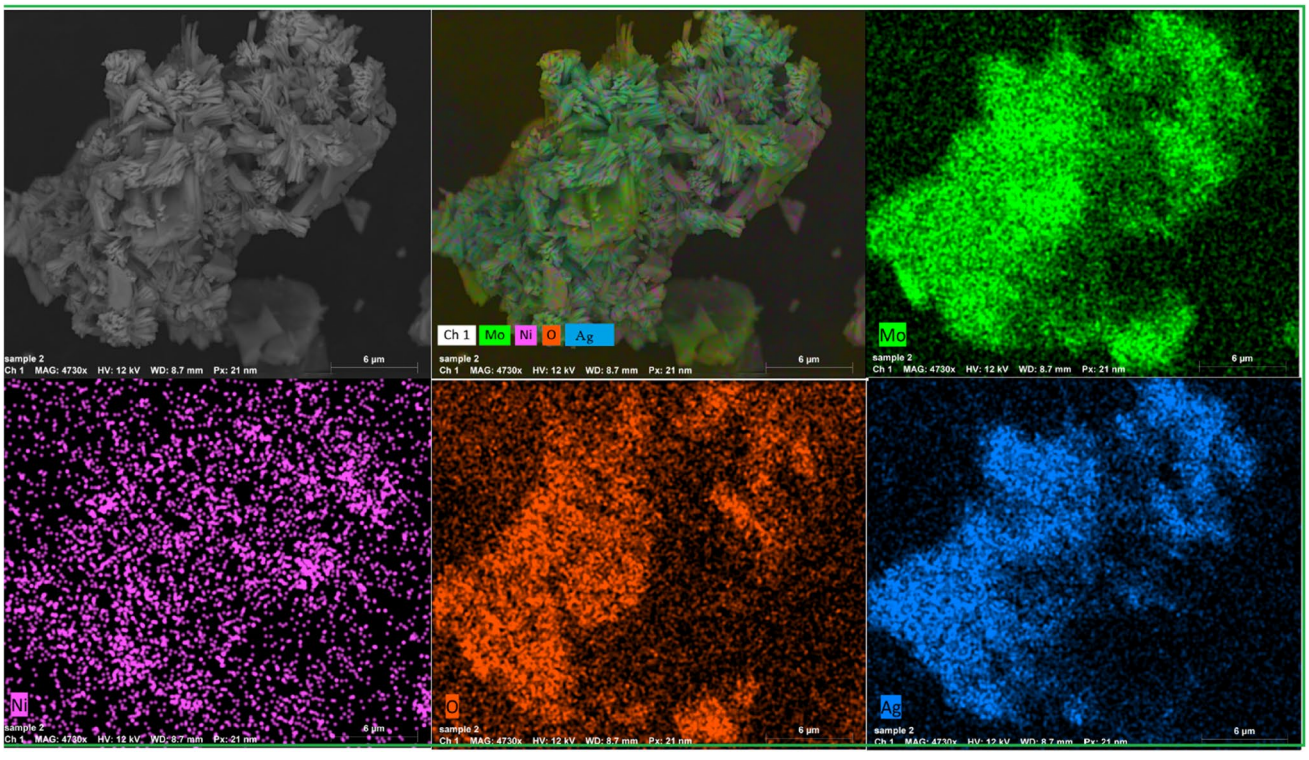

Fig. 5 Represents the SEM and elemental mapping images of Ag@NMO NPs

3.2 Antimicrobial Potential of Pure NMO NPs and Ag Modified-NMO NPs

The well diffusion experiment was performed to evaluate the antimicrobial performance of pure NMO NPs, and Ag@NMO NPs where Amoxicillin (AX) had been used as a positive antibacterial control against *S. sciuri*, *S. aureus*, *E. columbae*, *S. lentus*, and *S. vitulinus* and Nystatin (NS) had been used as a positive antifungal control upon *C. albicans*, and *C. tropicalis* as presented in Table 1 and Fig. 6.

The results revealed that both pure NMO NPs and Ag@NMO NPs express antimicrobial action toward

Table 1 The antimicrobial activity (ZOI) and minimum inhibitory concentration (as µg/mL) of NMO NPs and Ag@NMO NPs

Microbial strains	Zone of inhibition (mm), and MIC (µg/mL)				
	ZOI of NMO NPs (mm)	MIC of NMO NPs (µg/mL)	ZOI of Ag@NMO NPs (mm)	MIC of Ag@ NMO NPs (µg/mL)	ZOI of Amoxicillin (AX) and Nystatin (NS) (mm)
Staphylococcus aureus	18.0 ± 0.707^{d}	3.130	25.5 ± 1.154^{c}	0.195	10.0 ± 1.077^{b}
Staphylococcus sciuri	16.5 ± 0.707^{e}	6.250	18.2 ± 1.527^{e}	3.130	8.0 ± 0.524^{d}
Staphylococcus lentus	13.5 ± 1.411^{f}	12.50	16.0 ± 0.577^{f}	6.250	9.0 ± 2.640^{c}
Staphylococcus vitulinus	25.8 ± 0.572^{a}	0.195	32.0 ± 0.577^{s}	0.097	12.0 ± 0.577^{a}
Enterococcus columbae	24.5 ± 1.251^{b}	0.390	33.3 ± 0.115^{a}	0.048	8.0 ± 0.115^{d}
Candida albicans	25.0 ± 0.572^{a}	0.195	30.8 ± 0.572^{b}	0.097	8.0 ± 0.115^{d}
Candida tropicalis	20.0 ± 1.251^{c}	1.560	21.2 ± 1.251^{d}	0.780	9.0 ± 0.115^{c}

Values are means ± SD (n = 3). Data within the groups are analyzed using a one-way analysis of variance (ANOVA) followed by $^{a, b, c, d, e, f}$ Duncan's multiple range test (DMRT), Amoxicillin; standard antibacterial agent, Nystatin; standard antifungal agent (positive control)

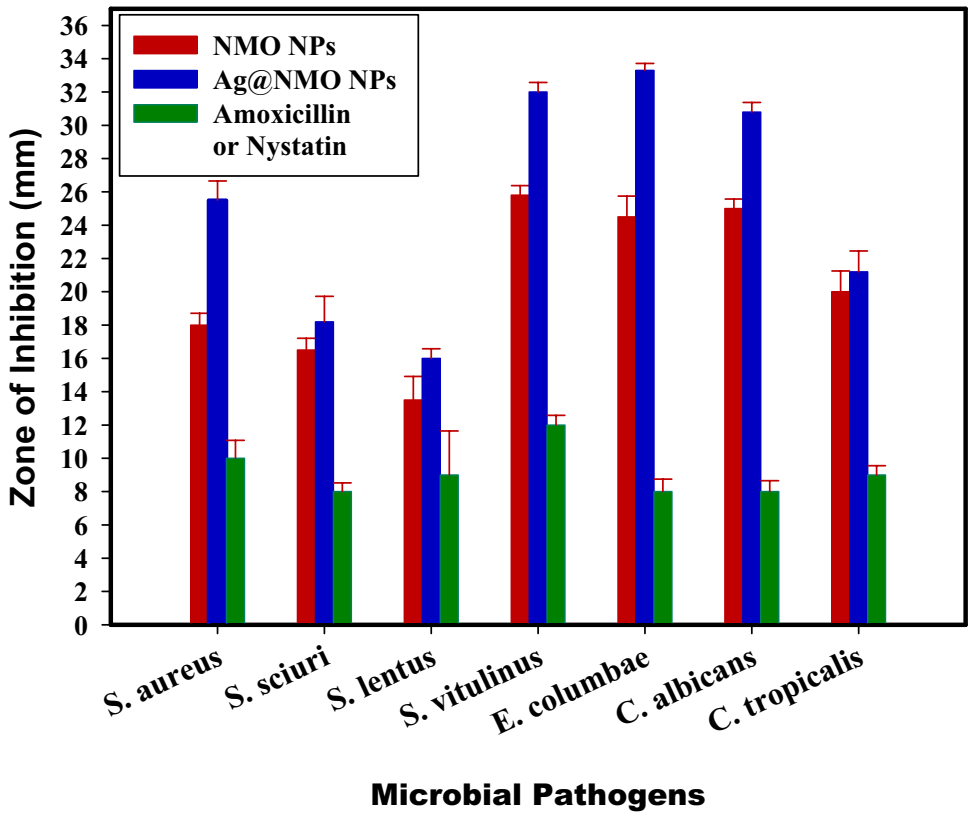

Fig. 6 Antimicrobial activity as ZOI for NMO NPs, and Ag@NMO NPs against different pathogenic bacteria and unicellular fungi

the examined pathogenic bacteria and *Candida* species. Additionally, the potential antimicrobial progress with the treatments, including silver. Accordingly, Ag@NMO NPs reported the most significant ZOI against *E. columbae* (33.3 ± 0.115 mm), and *C. albicans* (30.8 ± 0.572 mm) which was mainly influenced by Ag@NMO NPs.

3.3 MIC Investigation

MIC testing of pure NMO NPs and Ag@NMO NPs were studied. This analysis was carried out on pure NMO NPs, and Ag@NMO NPs at various concentrations of (as µg/mL) performing well diffusion method [78], and the results have been included in Table 1. MIC results are diversely proportional

with the potential of the tested treatment as antimicrobial action. The lowest MIC concentration of pure MNO NPs was recorded at 12.5 µg/mL upon *S. lentus*. As matched with well diffusion method results, Ag@NMO NPs were a further efficient antimicrobial factor than NMO NPs so, the MIC results in the presence of Ag were lower than pure NMO NPs. At the same time, Ag@NMO NPs showed the lowest MIC concentration. In Ag@NMO NPs, MIC concentration was low against *E. columbae* (0.048 µg/mL). Ag@NMO NPs have double function working as bacteriostatic in low concentration, on the other hand, acting as bactericidal at the high concentration [79].

3.4 Antibiofilm Activity of Pure NMO NPs and Ag Modified-NMO NPs

Pure NMO NPs and Ag@NMO NPs were adopted to assess their potency to restrain the examined bacterial strains' biofilm development and *Candida* species. About 0.5 mL of pure NMO NPs or Ag@NMO NPs were mixed into the tubes, including 5.0 mL of the nutrient broth injected with 10 µL of 0.5 McFarland ($1–3\times10^8$ CFU/mL) of the tested bacteria and unicellular fungi. At the same time, the equivalent volume of sterile distilled water was attached to the negative control tubes. It was pointed in Fig. 7 that Ag@NMO NPs was more effective in inhibiting the biofilm of all the examined bacteria and unicellular fungi preferably than pure NMO NPs.

The antibiofilm potential of Ag@NMO NPs was the most powerful, recording 94.32% for *E. columbae*, 91.99% for *S. vitulinus*, and 90.98% for *C. albicans* (Table 2). Since the antimicrobial potency of NPs effectively depends on the quantity of the particles, the small size of Ag@NMO NPs produces strong antibiofilm potential to the bacteria and unicellular fungi. It had known that biofilms are the effect of a general disease, and around 80% of bacterial infections in the world had combined with biofilms formation [80]. The ecological specifications and appearance of particular genes generated by adhesion may probably manage biofilms' metabolic activity [81]. The environmental requirements and expression of particular genes produced by adhesion may theoretically control biofilms' metabolic action. [82]. The low cellular metabolism preserves the antimicrobial agents that improve within bacterial extension [83].

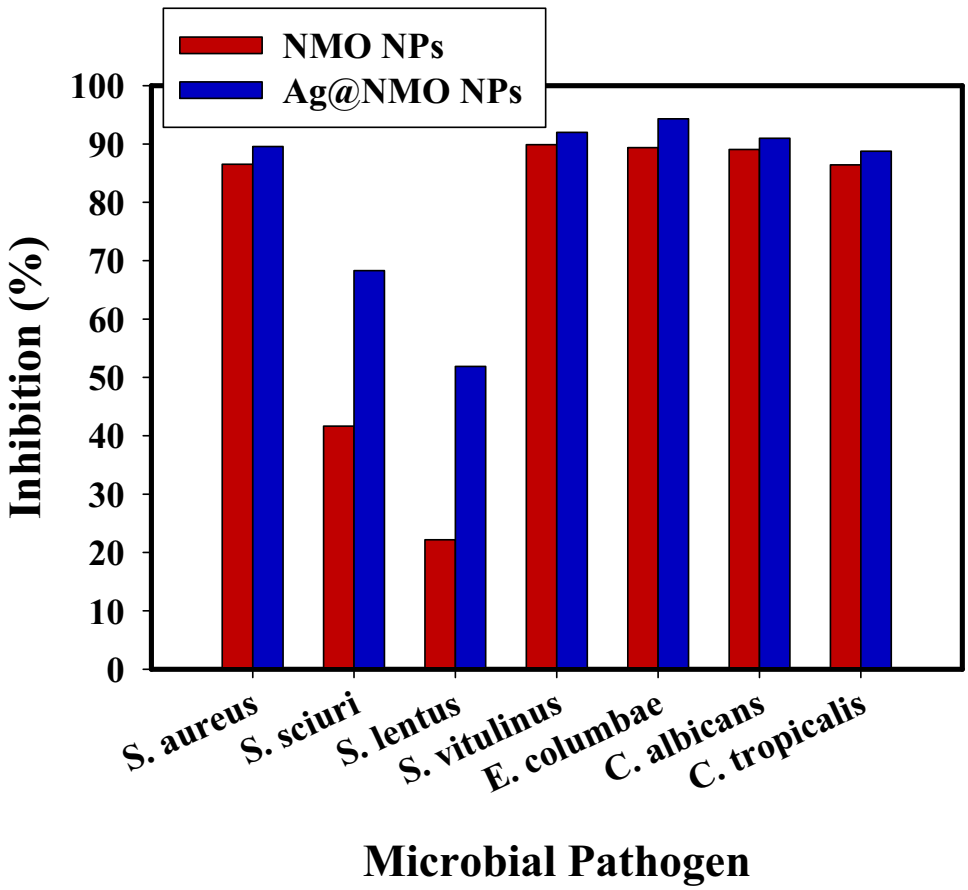

Fig. 7 Anbiofilm activity as inhibition % for NMO NPs, and Ag@NMO NPs against different pathogenic bacteria and unicellular fungi

Table 2 Semi-quantitative inhibition% of the biofilm formation for non-treated and treated bacterial and yeast pathogens with NMO NPs, and Ag@NMO NPs

Microbial strains	O.D. of crystal violet stain at 570.0 nm			Inhibition %	
	Control	NMO NPs	Ag@NMO NPs	NMO NPs	Ag@NMO NPs
Staphylococcus aureus	$0.958^{d} \pm 0.0080$	$0.129^{c} \pm 0.0021$	$0.100^{c} \pm 0.0062$	86.53	89.56
Staphylococcus sciuri	$1.025^{a} \pm 0.0062$	$0.598^{e} \pm 0.0047$	$0.325^{e} \pm 0.0047$	41.65	68.29
Staphylococcus lentus	$1.154^{b} \pm 0.0070$	$0.898^{b} \pm 0.0053$	$0.555^{b} \pm 0.0036$	22.18	51.90
Staphylococcus vitulinus	$0.999^{f} \pm 0.0025$	$0.101^{d} \pm 0.0062$	$0.080^{d} \pm 0.0053$	89.88	91.99
Enterococcus columbae	$1.215^{e} \pm 0.0046$	$0.129^{a} \pm 0.0036$	$0.069^{a} \pm 0.0062$	89.38	94.32
Candida albicans	$0.998^{cd} \pm 0.0046$	$0.109^{e} \pm 0.0036$	$0.090^{e} \pm 0.0047$	89.07	90.98
Candida tropicalis	$0.898^{cd} \pm 0.0046$	$0.122^{cd} \pm 0.0046$	$0.101^{cd} \pm 0.0046$	86.41	88.75

Values are means ± SD (n = 3). Data within the groups are analyzed using one-way analysis of variance (ANOVA) followed by $^{a, b, c, d, e, f}$ Duncan's multiple range test (DMRT)

3.5 Reaction Mechanism Determination by SEM Analysis

SEM examination was carried out to demonstrate the possible antimicrobial reaction mechanism against *E. columbae*, as observed in Fig. 8. The SEM examination of the control untreated *E. columbae* in the absence of Ag modified-NMO NPs showed bacterial accumulations that had normally grown with regular appearance. The usual bacterial surface and semi-developed biofilm had been observed (Fig. 8a). Simultaneous Ag@NMO NPs treatment, morphological alterations had been discovered in *E. columbae* (Fig. 8b), such as the complete lysis of the exterior surface accompanied by deformations and malformation of the *E. columbae* cells with the decrease in the total viable number, and the biofilm extension was restricted.

The schematic design presented in Fig. 9 exhibits the possible antibacterial mechanism. It must be understood that Ag@NMO NPs start their action with adhesion at the outer surface of the bacterial cell, causing membrane damage and alter the transport flow. Then, the diffusion of Ag^{+} in the bacterial cell (at pH = 3) and interacting with all intracellular structures such as a plasmid, DNA, and other necessary organelles. Ultimately, cellular and genetic toxicity occurs because of the oxidative tension created by reactive oxygen species (ROS) production. Finally, NMO NPs have resisted

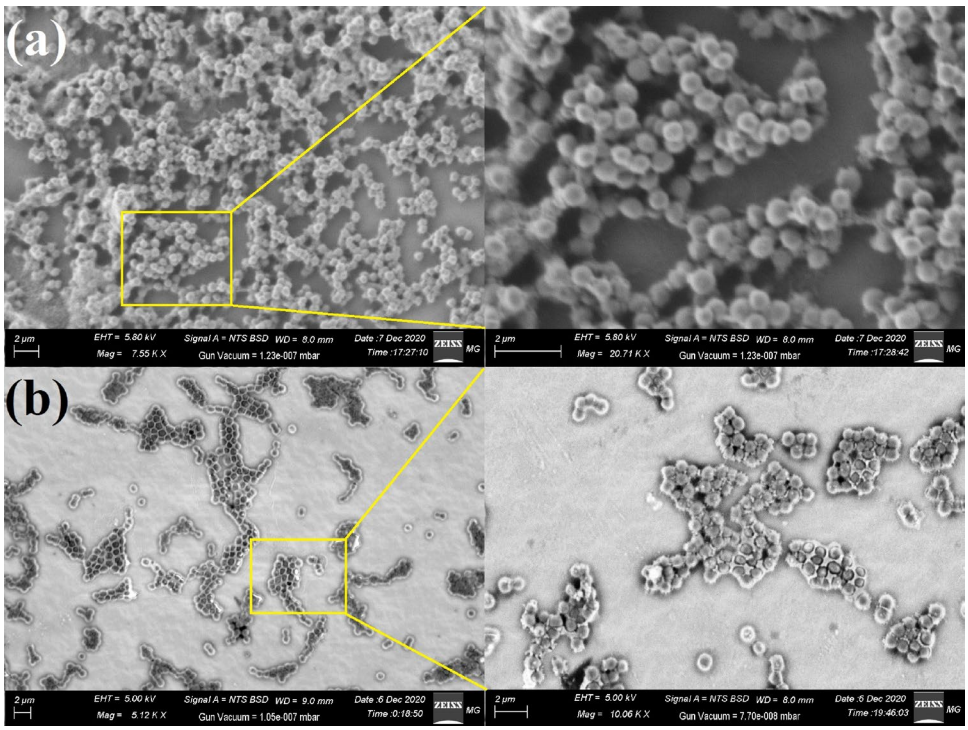

Fig. 8 SEM imaging of *E. columbae*; where **a** regular bacterial cells without Ag@NMO NPs treatment, **b** abnormal, deformed and irregular bacterial cell with complete lysis following Ag@NMO NPs treatment, fully-irregular and deformed bacterial cell through Ag@NMO NPs treatment presenting the full lysis of *E. columbae* cell, and malformed bacterial cell after the treatment of Ag@NMO NPs

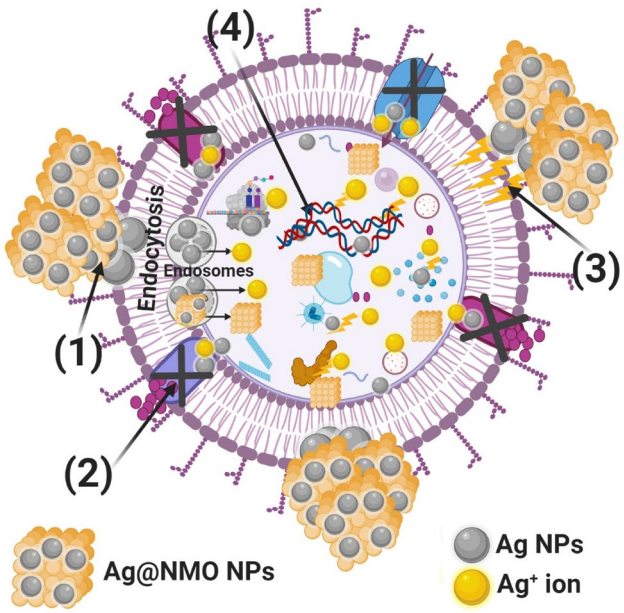

Fig. 9 Schematic representation regarding the four prominent ways of antibacterial potential of Ag@NMO NPs, where (1) Ag@NMO NPs adhere to the bacterial cell surface and results in membrane damage and altered transport activity; (2) Ag@NMO NPs block the ions transport from and to the bacterial cell, (3) Ag@NMO NPs create and increase the ROS leading to bacterial cell wall damage, and (4) Ag@NMO NPs penetrate inside the bacterial cells and interact with cellular organelles and biomolecules, and thereby, affect respective cellular machinery, and modulate the cellular signal system and causing cell death. Ag@NMO NPs may serve as a vehicle to effectively-deliver Ag^+ ions to the bacterial cytoplasm and membrane, where proton motive force would decrease the pH to be less than 3.0 and therefore improve the release of Ag^+ ions

the bacterial cells' acidic environment, and the transfer did not happen [64], but kept the antibacterial potential by altering the signal transduction mechanisms [84].

4 Conclusion

For the first time, this work exhibits that gamma irradiation supported the sol–gel structure of Ag modified-NMO NPs. The XRD established the strong development of Ag@NMO NPs. Also, the EDX spectra confirmed that the fundamental elements were uniformly distributed within the Ag@NMO NPs without any foreign particles, which declared the purity of the Ag@NMO NPs. Also, the HR-TEM image shows that the particles of NMO possess a hexagonal shape in the nanoscale regime. Ag modified-NMO NPs was the well-known decisive antimicrobial activity towards all the tested pathogenic bacteria and unicellular fungi. The capability of Ag@NMO NPs decreases in the following form *E. columbae* (33.3 mm) > *S. vitulinus* (32.0 mm) > *C. albicans* (30.8 mm) > *S. aureus* (25.5 mm) > *C. tropicalis* (21.2 nm) > *S. sciuri* (18.2 nm) > *S. lentus* (16.0 nm). In Ag@NMO NPs, MIC concentration was low upon *E. columbae* (0.048 µg/ml). The antibiofilm potential of Ag@NMO NPs was the most powerful, recording 94.32% for *E. columbae*, 91.99% for *S. vitulinus*, and 90.98% for *C. albicans*. Since the antimicrobial strength of NPs dramatically depends on the particles size, the small size of Ag@NMO NPs provides effective antibiofilm behavior against the tested bacteria and unicellular fungi. It had recommended that Ag modified-NMO NPs replace some disinfectant liquids used for the surface disinfection in hospitals and some colors in the medical operating offices to protect the environment from entering the pathogenic bacteria. Furthermore, Ag modified-NMO NPs may have been acquired as a component in medical cosmetics and pharmaceuticals for biomedical approaches. Finally, Ag modified-NMO NPs may be employed in construction and environmental goals like rainwater processing from the contaminants and protect the atmosphere from deadly pathogens and dangerous diseases.

Supplementary Information The online version contains supplementary material available at https://doi.org/10.1007/s10904-021-02132-9.

Acknowledgements The authors would like to thank the Deanship of Scientific Research at Taif University for funding this work through Taif University Researchers Supporting Project number (TURSP-2020/220), Taif University, Taif, Saudi Arabia.

Author Contributions MIAAM, conceptualizing, refining research idea, creating research design, manuscript writing, editing, figures designing and drawing; GSES, conceptualizing, refining research idea, creating research design, manuscript writing, editing, figures designing and drawing. EF, manuscript writing, and editing; AA, manuscript writing, and editing; OAAA, manuscript writing; and editing; AAE, manuscript writing, editing, figures designing and drawing.

Funding The current work was funded by Taif University Researchers Supporting Project number (TURSP-2020/220), Taif University, Taif, Saudi Arabia.

Data Availability Not applicable.

Declarations

Conflict of interest All authors declare no conflict of interest.

Ethical Approval Not applicable.

Informed Consent Not applicable.

Research Involving Human Participation and/or Animals Not applicable.

References

1. M. Abd Elkodous, G.S. El-Sayyad, H.A. Nasser, A.A. Elshamy, M. Morsi, I.Y. Abdelrahman, A.S. Kodous, F.M. Mosallam, M. Gobara, A.I. El-Batal, Engineered nanomaterials as potential candidates for HIV treatment: between opportunities and challenges. J. Clust. Sci. **30**(3), 531–540 (2019)
2. M. Abd Elkodous, G.S. El-Sayyad, M.M. Abdel-Daim, Engineered nanomaterials as fighters against SARS-CoV-2: the way to control and treat pandemics. Environ. Sci. Pollut. Res. **28**(30), 40409–40415 (2021)
3. W.P. Gilks, P.M. Abou-Sleiman, S. Gandhi, S. Jain, A. Singleton, A.J. Lees, K. Shaw, K.P. Bhatia, V. Bonifati, N.P. Quinn, J. Lynch, D.G. Healy, J.L. Holton, T. Revesz, N.W. Wood, A common LRRK2 mutation in idiopathic Parkinson's disease. Lancet **365**(9457), 415–416 (2005)
4. K.H. Mayer, C.L. Karp, P.G. Auwaerter, K.H. Mayer, Coinfection with HIV and tropical infectious diseases. I. Protozoal pathogens. Clin. Infect. Dis. **45**(9), 1208–1213 (2007)
5. N. Kaplowitz, Idiosyncratic drug hepatotoxicity. Nat. Rev. Drug Discov. **4**(6), 489 (2005)
6. C.D. Stehouwer, J. Lambert, A. Donker, V.W. van Hinsbergh, Endothelial dysfunction and pathogenesis of diabetic angiopathy. Cardiovasc. Res. **34**(1), 55–68 (1997)
7. G.S. El-Sayyad, F.M. Mosallam, A.I. El-Batal, One-pot green synthesis of magnesium oxide nanoparticles using *Penicillium chrysogenum* melanin pigment and gamma rays with antimicrobial activity against multidrug-resistant microbes. Adv. Powder Technol. **29**(11), 2616–2625 (2018)
8. R.J. Fair, Y. Tor, Antibiotics and bacterial resistance in the 21st century. Perspect. Med. Chem. (2014). https://doi.org/10.4137/PMC.S14459
9. Y. Liu, H. Miyoshi, M. Nakamura, Nanomedicine for drug delivery and imaging: a promising avenue for cancer therapy and diagnosis using targeted functional nanoparticles. Int. J. Cancer **120**(12), 2527–2537 (2007)
10. A. Ashour, A.I. El-Batal, M.A. Maksoud, G.S. El-Sayyad, S. Labib, E. Abdeltwab, M. El-Okr, Antimicrobial activity of metal-substituted cobalt ferrite nanoparticles synthesized by sol–gel technique. Particuology **40**, 141–151 (2018)
11. M.-C. Daniel, D. Astruc, Gold nanoparticles: assembly, supramolecular chemistry, quantum-size-related properties, and applications toward biology, catalysis, and nanotechnology. Chem. Rev. **104**(1), 293–346 (2004)
12. J. Jeevanandam, A. Barhoum, Y.S. Chan, A. Dufresne, M.K. Danquah, Review on nanoparticles and nanostructured materials: history, sources, toxicity and regulations. Beilstein J. Nanotechnol. **9**, 1050–1074 (2018)
13. K. Pal, S. Sajjadifar, M.A. Elkodous, Y.A. Alli, F. Gomes, J. Jeevanandam, S. Thomas, A. Sigov, Soft, self-assembly liquid crystalline nanocomposite for superior switching. Electron. Mater. Lett. **15**(1), 84–101 (2019)
14. A.I. El-Batal, N.M. Sidkey, A. Ismail, R.A. Arafa, R.M. Fathy, Impact of silver and selenium nanoparticles synthesized by gamma irradiation and their physiological response on early blight disease of potato. J. Chem. Pharm. Res **8**(4), 934–951 (2016)
15. A. El-Batal, B.M. Haroun, A.A. Farrag, A. Baraka, G.S. El-Sayyad, Synthesis of silver nanoparticles and incorporation with certain antibiotic using gamma irradiation. Br. J. Pharm. Res. **4**(11), 1341 (2014)
16. M. Abd Elkodous, G.S. El-Sayyad, M.I.A. Abdel Maksoud, I.Y. Abdelrahman, F.M. Mosallam, M. Gobara, A.I. El-Batal, Fabrication of ultra-pure anisotropic zinc oxide nanoparticles via simple and cost-effective route: implications for UTI and EAC medications. Biol. Trace Elem. Res. **196**(1), 297–317 (2020)
17. A.I. El-Batal, F.M. Mosalam, M. Ghorab, A. Hanora, A.M. Elbarbary, Antimicrobial, antioxidant and anticancer activities of zinc nanoparticles prepared by natural polysaccharides and gamma radiation. Int. J. Biol. Macromol. **107**, 2298–2311 (2018)
18. A.I. El-Batal, G.S. El-Sayyad, A. El-Ghamry, K.M. Agaypi, M.A. Elsayed, M. Gobara, Melanin-gamma rays assistants for bismuth oxide nanoparticles synthesis at room temperature for enhancing antimicrobial, and photocatalytic activity. J. Photochem. Photobiol. B **173**, 120–139 (2017)
19. M.I.A. Abdel Maksoud, R.A. Fahim, A.E. Shalan, M. Abd Elkodous, S.O. Olojede, A.I. Osman, C. Farrell, A.A.H. Al-Muhtaseb, A.S. Awed, A.H. Ashour, D.W. Rooney, Advanced materials and technologies for supercapacitors used in energy conversion and storage: a review. Environ. Chem. Lett. **19**(1), 375–439 (2021)
20. M. Wu, J. Shi, Beneficial and detrimental impacts of molybdate on corrosion resistance of steels in alkaline concrete pore solution with high chloride contamination. Corros. Sci. **183**, 109326 (2021)
21. T. Ghiasi, S. Ahmadi, E. Ahmadi, M.R.T. Bavil Olyai, Z. Khodadadi, Novel electrochemical sensor based on modified glassy carbon electrode with graphene quantum dots, chitosan and nickel molybdate nanocomposites for diazinon and optimal design by the Taguchi method. Microchem. J. **160**, 105628 (2021)
22. G. Yang, Y. Liang, K. Li, J. Yang, K. Wang, R. Xu, X. Xie, Engineering the dimension and crystal structure of bismuth molybdate photocatalysts via a molten salt-assisted assembly approach. J. Alloys Compd. **844**, 156231 (2020)
23. Z. Xia, J. Min, S. Zhou, H. Ma, B. Zhang, X. Tang, Photocatalytic performance and antibacterial mechanism of Cu/Ag-molybdate powder material. Ceram. Int. **47**(9), 12667–12679 (2021)
24. S.P. Keerthana, B.J. Rani, R. Yuvakkumar, G. Ravi, Y. Shivatharsiny, E.S. Babu, H.S. Almoallim, S.A. Alharbi, D. Velauthapillai, Copper molybdate nanoparticles for electrochemical water splitting application. Int. J. Hydrog. Energy **46**(11), 7701–7711 (2021)
25. B. Ramulu, S. Chandra Sekhar, G. Nagaraju, J.S. Yu, Rational design and construction of nickel molybdate nanohybrid composite for high-performance supercapattery. Appl. Surf. Sci. **515**, 146023 (2020)
26. C. Karami, M.A. Taher, A novel enzyme-less amperometric sensor for hydrogen peroxide based on nickel molybdate nanoparticles. J. Electroanal. Chem. **847**, 113219 (2019)
27. W. Zhang, J. Yin, F. Min, L. Jia, D. Zhang, Q. Zhang, J. Xie, Preparation and photoluminescence properties of MMoO4 (M = Cu, Ni, Zn) nano-particles synthesized via electrolysis. J. Mol. Struct. **1127**, 777–783 (2017)
28. V. Umapathy, P. Neeraja, A. Manikandan, P. Ramu, Synthesis of NiMoO4 nanoparticles by sol–gel method and their structural, morphological, optical, magnetic and photocatlytic properties. Trans. Nonferrous Metal. Soci. China **27**(8), 1785–1793 (2017)
29. A. Alborzi, S. Khademolhoseini, Nickel molybdate nanoparticles: synthesis, characterization, optical and photocatalytic properties. J. Mater. Sci.: Mater. Electron. **27**(4), 3963–3967 (2016)
30. R. Salomoni, P. Léo, A. Montemor, B. Rinaldi, M. Rodrigues, Antibacterial effect of silver nanoparticles in Pseudomonas aeruginosa. Nanotechnol. Sci. Appl. **10**, 115 (2017)
31. S. Park, H.H. Park, S.Y. Kim, S.J. Kim, K. Woo, G. Ko, Antiviral properties of silver nanoparticles on a magnetic hybrid colloid. Appl. Environ. Microbiol. **80**(8), 2343–2350 (2014)
32. N.T. Khan, M. Mushtaq, Determination of antifungal activity of silver nanoparticles produced from *Aspergillus niger*. Biol. Med. **9**(1), 1 (2017)
33. G. Kannayiram, A. Sandhya, S. Sowmiya, S. Valarmathi, D. Joseph, Anti-inflammatory activity of nigella sativa silver

nanoparticles: biochemical study. Asian J. Pharm. Clin. Res. (2019). https://doi.org/10.22159/ajpcr.2019.v12i2.29775
34. S. Yesilot, C. Aydin, Silver nanoparticles; a new hope in cancer therapy? East. J. Med. **24**(1), 111–116 (2019)
35. K. Venugopal, H. Rather, K. Rajagopal, M. Shanthi, K. Sheriff, M. Illiyas, R. Rather, E. Manikandan, S. Uvarajan, M. Bhaskar, Synthesis of silver nanoparticles (Ag NPs) for anticancer activities (MCF 7 breast and A549 lung cell lines) of the crude extract of *Syzygium aromaticum*. J. Photochem. Photobiol. B **167**, 282–289 (2017)
36. M. Abd Elkodous, G.S. El-Sayyad, I.Y. Abdelrahman, H.S. El-Bastawisy, A.E. Mohamed, F.M. Mosallam, H.A. Nasser, M. Gobara, A. Baraka, M.A. Elsayed, A.I. El-Batal, Therapeutic and diagnostic potential of nanomaterials for enhanced biomedical applications. Colloids Surf. B **180**, 411–428 (2019)
37. C.W. Wong, Y.S. Chan, J. Jeevanandam, K. Pal, M. Bechelany, M. Abd Elkodous, G.S. El-Sayyad, Response surface methodology optimization of mono-dispersed MgO nanoparticles fabricated by ultrasonic-assisted sol-gel method for outstanding antimicrobial and antibiofilm activities. J. Clust. Sci. **31**(2), 367–389 (2020)
38. G.S. El-Sayyad, M. Abd Elkodous, A.M. El-Khawaga, M.A. Elsayed, A.I. El-Batal, M. Gobara, Merits of photocatalytic and antimicrobial applications of gamma-irradiated $Co_xNi_{1-x}Fe_2O_4$/SiO_2/TiO_2; x = 0.9 nanocomposite for pyridine removal and pathogenic bacteria/fungi disinfection: implication for wastewater treatment. RSC Adv. **10**(9), 5241–5259 (2020)
39. M.M. Atta, M.I.A. Abdel Maksoud, O.I. Sallam, A.S. Awed, Gamma irradiation synthesis of wearable supercapacitor based on reduced graphene oxide/cotton yarn electrode. J. Mater. Sci.: Mater. Electron. **32**(3), 3688–3698 (2021)
40. M. Bekhit, A.O. Abo El Naga, M. El Saied, M.I.A. Abdel Maksoud, Radiation-induced synthesis of copper sulfide nanotubes with improved catalytic and antibacterial activities. Environ. Sci. Pollut. Res. (2021). https://doi.org/10.1007/s11356-021-13482-9
41. G.G. Flores-Rojas, F. López-Saucedo, E. Bucio, Gamma-irradiation applied in the synthesis of metallic and organic nanoparticles: a short review. Radiat. Phys. Chem. **169**, 107962 (2020)
42. Z.I. Ali, M. Bekhit, R. Sokary, T.A. Afify, Radiation synthesis of copper sulphide/poly(vinyl alcohol) nanocomposites films: an efficient and reusable catalyst for p-nitrophenol reduction. Int. J. Environ. Anal. Chem. **99**(13), 1313–1324 (2019)
43. M.I.A. Abdel Maksoud, G.S. El-Sayyad, H.S. El-Bastawisy, R.M. Fathy, Antibacterial and antibiofilm activities of silver-decorated zinc ferrite nanoparticles synthesized by a gamma irradiation-coupled sol–gel method against some pathogenic bacteria from medical operating room surfaces. RSC Adv. **11**(45), 28361–28374 (2021)
44. M.I.A.A. Maksoud, G.S. El-Sayyad, A.H. Ashour, A.I. El-Batal, M.A. Elsayed, M. Gobara, A.M. El-Khawaga, E.K. Abdel-Khalek, M.M. El-Okr, Antibacterial, antibiofilm, and photocatalytic activities of metals-substituted spinel cobalt ferrite nanoparticles. Microb. Pathog. **127**, 144–158 (2019)
45. M.I.A. Abdel Maksoud, G.S. El-Sayyad, A.H. Ashour, A.I. El-Batal, M.S. Abd-Elmonem, H.A.M. Hendawy, E.K. Abdel-Khalek, S. Labib, E. Abdeltwab, M.M. El-Okr, Synthesis and characterization of metals-substituted cobalt ferrite [M_x $Co_{(1-x)}$ Fe_2O_4; (M = Zn, Cu and Mn; x = 0 and 0.5)] nanoparticles as antimicrobial agents and sensors for Anagrelide determination in biological samples. Mater. Sci. Eng. **92**, 644–656 (2018)
46. M.I.A.A. Maksoud, A. El-ghandour, G.S. El-Sayyad, A.S. Awed, R.A. Fahim, M.M. Atta, A.H. Ashour, A.I. El-Batal, M. Gobara, E.K. Abdel-Khalek, M.M. El-Okr, Tunable structures of copper substituted cobalt nanoferrites with prospective electrical and magnetic applications. J. Mater. Sci.: Mater. Electron. **30**(5), 4908–4919 (2019)
47. M.I.A. Abdel Maksoud, A. El-ghandour, G.S. El-Sayyad, A.S. Awed, A.H. Ashour, A.I. El-Batal, M. Gobara, E.K. Abdel-Khalek, M.M. El-Okr, Incorporation of Mn^{2+} into cobalt ferrite via sol–gel method: insights on induced changes in the structural, thermal, dielectric, and magnetic properties. J. Sol-Gel Sci. Technol. **90**(3), 631–642 (2019)
48. S. Cong, T. Sugahara, T. Wei, J. Jiu, Y. Hirose, S. Nagao, K. Suganuma, Growth and extension of one-step sol-gel derived molybdenum trioxide nanorods via controlling citric acid decomposition rate. Cryst. Growth Des. **15**(9), 4536–4542 (2015)
49. A. Kaddouri, E. Tempesti, C. Mazzocchia, Comparative study of β-nickel molybdate phase obtained by conventional precipitation and the sol-gel method. Mater. Res. Bull. **39**(4), 695–706 (2004)
50. S. Balasurya, A. Syed, L.L. Raju, S. Al-Rashed, A.M. Thomas, A. Das, S.S. Khan, Elucidation of photocatalysis, photoluminescence and antibacterial studies of Ag2MoO4 decorated NiMoO4 nano-heterostructure. Opt. Mater. **113**, 110856 (2021)
51. M.I.A. Abdel Maksoud, A.S. Awed, R. Sokary, M. Bekhit, Effect of gamma irradiation on the free-standing polyvinyl alcohol/chitosan/Ag nanocomposite films: insights on the structure, optical, and dispersion properties. Appl. Phys. A **127**(8), 619 (2021)
52. M.I.A. Abdel Maksoud, M.M. Ghobashy, G.S. El-Sayyad, A.M. El-Khawaga, M.A. Elsayed, A.H. Ashour, Gamma irradiation-assisted synthesis of PANi/Ag/MoS_2/$LiCo_{0.5}Fe_2O_4$ nanocomposite: efficiency evaluation of photocatalytic bisphenol A degradation and microbial decontamination from wastewater. Opt. Mater. **119**, 111396 (2021)
53. A.A. Reheem, A. Atta, M.A. Maksoud, Low energy ion beam induced changes in structural and thermal properties of polycarbonate. Radiat. Phys. Chem. **127**, 269–275 (2016)
54. P. Belavi, G. Chavan, L. Naik, R. Somashekar, R. Kotnala, Structural, electrical and magnetic properties of cadmium substituted nickel–copper ferrites. Mater. Chem. Phys. **132**(1), 138–144 (2012)
55. M.K. Abdel-Rafei, N.M. Thabet, M. Abdel Maksoud, M. Abd Elkodous, G. Kawamura, A. Matsuda, A. Ashour, A.I. El-Batal, G.S. El-Sayyad, Influence of Ce^{3+} substitution on antimicrobial and antibiofilm properties of $ZnCe_xFe_{2-x}O_4$ nanoparticles (X= 0.0, 0.02, 0.04, 0.06, and 0.08) conjugated with ebselen and its role subsidised with γ-radiation in mitigating human TNBC and colorectal adenocarcinoma proliferation in vitro. Int. J. Mol. Sci. **22**(18), 10171 (2021)
56. A.I. El-Batal, G.S. El-Sayyad, F.M. Mosallam, R.M. Fathy, *Penicillium chrysogenum*-mediated mycogenic synthesis of copper oxide nanoparticles using gamma rays for in vitro antimicrobial activity against some plant pathogens. J. Clust. Sci. **31**(1), 79–90 (2020)
57. A.I. El-Batal, M.S. Attia, M.M. Nofel, G.S. El-Sayyad, Potential nematicidal properties of silver boron nanoparticles: synthesis, characterization, in vitro and in vivo root-knot nematode (*Meloidogyne incognita*) treatments. J. Clust. Sci. **30**(3), 687–705 (2019)
58. R.M. Fathy, M.S.E.-D. Salem, A.Y. Mahfouz, Biogenic synthesis of silver nanoparticles using *Gliocladium deliquescens* and their application as household sponge disinfectant. Biol. Trace Elem. Res. **196**(2), 662–678 (2020)
59. M.I.A. Abdel Maksoud, G.S. El-Sayyad, A. Abokhadra, L.I. Soliman, H.H. El-Bahnasawy, A.H. Ashour, Influence of Mg^{2+} substitution on structural, optical, magnetic, and antimicrobial properties of Mn–Zn ferrite nanoparticles. J. Mater. Sci.: Mater. Electron. **31**(3), 2598–2616 (2020)
60. K.F. El-Nemr, H.R. Mohamed, M.A. Ali, R.M. Fathy, A.S. Dhmees, Polyvinyl alcohol/gelatin irradiated blends filled by lignin as green filler for antimicrobial packaging materials. Int. J. Environ. Anal. Chem. **100**(14), 1578–1602 (2020)

61. A.I. El-Batal, H.G. Nada, R.R. El-Behery, M. Gobara, G.S. El-Sayyad, Nystatin-mediated bismuth oxide nano-drug synthesis using gamma rays for increasing the antimicrobial and antibiofilm activities against some pathogenic bacteria and *Candida* species. RSC Adv. **10**(16), 9274–9289 (2020)
62. A.M. El-Khawaga, A.A. Farrag, M.A. Elsayed, G.S. El-Sayyad, A.I. El-Batal, Antimicrobial and photocatalytic degradation activities of chitosan-coated magnetite nanocomposite. J. Clust. Sci. **32**(5), 1107–1119 (2021)
63. K.F. El-Nemr, H.R. Mohamed, M.A. Ali, R.M. Fathy, A.S. Dhmees, Polyvinyl alcohol/gelatin irradiated blends filled by lignin as green filler for antimicrobial packaging materials. Int. J. Environ. Anal. Chem. **100**, 1–25 (2019)
64. A.N. El-Shazly, G.S. El-Sayyad, A.H. Hegazy, M.A. Hamza, R.M. Fathy, E. El Shenawy, N.K. Allam, Superior visible light antimicrobial performance of facet engineered cobalt doped TiO_2 mesocrystals in pathogenic bacterium and fungi. Sci. Rep. **11**(1), 1–14 (2021)
65. M. Abd Elkodous, G.S. El-Sayyad, S.M. Youssry, H.G. Nada, M. Gobara, M.A. Elsayed, A.M. El-Khawaga, G. Kawamura, W.K. Tan, A.I. El-Batal, Carbon-dot-loaded Co_xNi_{1-x} Fe_2O_4; x= 0.9/SiO_2/TiO_2 nanocomposite with enhanced photocatalytic and antimicrobial potential: An engineered nanocomposite for wastewater treatment. Sci. Rep. **10**(1), 1–22 (2020)
66. J. Yesuraj, O. Padmaraj, S.A. Suthanthiraraj, Synthesis, characterization, and improvement of supercapacitor properties of NiMoO4 nanocrystals with polyaniline. J. Inorg. Organomet. Polym. Mater. **30**(2), 310–321 (2020)
67. M. Kumar, R. Singh, H. Khajuria, H.N. Sheikh, Facile hydrothermal synthesis of nanocomposites of nitrogen doped graphene with metal molybdates (NG-MMoO 4)(M= Mn Co, and Ni) for enhanced photodegradation of methylene blue. J. Mater. Sci.: Mater. Electron. **28**(13), 9423–9434 (2017)
68. B. Senthilkumar, K.V. Sankar, R.K. Selvan, M. Danielle, M. Manickam, Nano α-NiMoO 4 as a new electrode for electrochemical supercapacitors. RSC Adv. **3**(2), 352–357 (2013)
69. B. Gauri, K. Vidya, D. Sharada, W. Shobha, Synthesis and characterization of Ag/AgO nanoparticles as alcohol sensor. Res. J. Chem. Environ. **20**(10), 1–5 (2016)
70. H. Yang, Y.-Y. Ren, T. Wang, C. Wang, Preparation and antibacterial activities of Ag/Ag+/Ag3+ nanoparticle composites made by pomegranate (*Punica granatum*) rind extract. Results Phys. **6**, 299–304 (2016)
71. S. Kumar Ray, D. Dhakal, G. Gyawali, B. Joshi, A. Raj Koirala, S. Wohn Lee, Transformation of tetracycline in water during degradation by visible light driven Ag nanoparticles decorated α-NiMoO4 nanorods: mechanism and pathways. Chem. Eng. J. **373**, 259–274 (2019)
72. J. Hu, Q. Liu, L. Shi, Z. Shi, H. Huang, Silver decorated LaMnO3 nanorod/graphene composite electrocatalysts as reversible metal-air battery electrodes. Appl. Surf. Sci. **402**, 61–69 (2017)
73. B. Alshahrani, H. ElSaeedy, A. Korna, H. Yakout, M.A. Maksoud, R.A. Fahim, M. Gobara, A. Ashour, The effect of Ce 3+ doping on structural, optical, ferromagnetic resonance, and magnetic properties of ZnFe 2 O 4 nanoparticles. J. Mater. Sci.: Mater. Electron. **32**(1), 780–797 (2021)
74. M.I.A. Abdel Maksoud, A. El-Ghandour, A.H. Ashour, M.M. Atta, S. Abdelhaleem, A.H. El-Hanbaly, R.A. Fahim, S.M. Kassem, M.S. Shalaby, A.S. Awed, La^{3+} doped $LiCo_{0.25}Zn_{0.25}Fe_2O_4$ spinel ferrite nanocrystals: insights on structural, optical and magnetic properties. J. Rare Earths **39**(1), 75–82 (2021)
75. P. Scherrer, Estimation of the size and internal structure of colloidal particles by means of röntgen. Nachr. Ges. Wiss. Göttingen **2**, 96–100 (1918)
76. U. Holzwarth, N. Gibson, The Scherrer equation versus the 'Debye-Scherrer equation.' Nat. Nanotechnol. **6**(9), 534–534 (2011)
77. M.I.A. Abdel Maksoud, A. El-Ghandour, G.S. El-Sayyad, R.A. Fahim, A.H. El-Hanbaly, M. Bekhit, E.K. Abdel-Khalek, H.H. El-Bahnasawy, M. Abd Elkodous, A.H. Ashour, A.S. Awed, Unveiling the effect of Zn^{2+} substitution in enrichment of structural, magnetic, and dielectric properties of cobalt ferrite. J. Inorg. Organometal. Polym. Mater. **30**(9), 3709–3721 (2020)
78. A.S. Awed, G.S. El-Sayyad, A. El-ghandour, M.F.O. Hameed, M.I.A. Abdel Maksoud, A.I. El-Batal, S.S.A. Obayya, Unveiling antimicrobial activity of metal iodide (CuI, AgI, and PbI_2) nanoparticles: towards biomedical surfaces applications. J. Clust. Sci. **32**(1), 1–16 (2021)
79. A.I. El-Batal, M. Abd Elkodous, G.S. El-Sayyad, N.E. Al-Hazmi, M. Gobara, A. Baraka, Gum Arabic polymer-stabilized and gamma rays-assisted synthesis of bimetallic silver-gold nanoparticles: powerful antimicrobial and antibiofilm activities against pathogenic microbes isolated from diabetic foot patients. Int. J. Biol. Macromol. **165**, 169–186 (2020)
80. J.C. Janssens, H. Steenackers, S. Robijns, E. Gellens, J. Levin, H. Zhao, K. Hermans, D. De Coster, T.L. Verhoeven, K. Marchal, Brominated furanones inhibit biofilm formation by *Salmonella enterica* serovar Typhimurium. Appl. Environ. Microbiol. **74**(21), 6639–6648 (2008)
81. R.M. Donlan, Biofilms: microbial life on surfaces. Emerg. Infect. Dis. **8**(9), 881 (2002)
82. W.M. Dunne, Bacterial adhesion: seen any good biofilms lately? Clin. Microbiol. Rev. **15**(2), 155–166 (2002)
83. M. Burmølle, J.S. Webb, D. Rao, L.H. Hansen, S.J. Sørensen, S. Kjelleberg, Enhanced biofilm formation and increased resistance to antimicrobial agents and bacterial invasion are caused by synergistic interactions in multispecies biofilms. Appl. Environ. Microbiol. **72**(6), 3916–3923 (2006)
84. A.I. El-Batal, N.M. Balabel, M.S. Attia, G.S. El-Sayyad, Antibacterial and antibiofilm potential of mono-dispersed stable copper oxide nanoparticles-streptomycin nano-drug: implications for some potato plant bacterial pathogen treatment. J. Clust. Sci. **31**, 1–20 (2019)